

UC Berkeley

UC Berkeley Previously Published Works

Title

Large emissions of CO₂ and CH₄ due to active-layer warming in Arctic tundra.

Permalink

<https://escholarship.org/uc/item/9nn7q74z>

Journal

Nature Communications, 16(1)

Authors

Torn, Margaret

Abramoff, Rose

Vaughn, Lydia

et al.

Publication Date

2025-01-02

DOI

10.1038/s41467-024-54990-9






Peer reviewed

Large emissions of CO₂ and CH₄ due to active-layer warming in Arctic tundra

Received: 6 March 2024

Accepted: 27 November 2024

Published online: 02 January 2025

 Check for updatesMargaret S. Torn ^{1,2}✉, Rose Z. Abramoff ^{1,3}, Lydia J. S. Vaughn ^{1,4},
Oriana E. Chafe ^{1,5}, J. Bryan Curtis¹ & Biao Zhu ^{1,6}

Climate warming may accelerate decomposition of Arctic soil carbon, but few controlled experiments have manipulated the entire active layer. To determine surface-atmosphere fluxes of carbon dioxide and methane under anticipated end-of-century warming, here we used heating rods to warm (by 3.8 °C) to the depth of permafrost in polygonal tundra in Utqiagvik (formerly Barrow), Alaska and measured fluxes over two growing seasons. We show that ecosystem respiration is ~30% higher in warmed plots than in control plots (0.99 $\mu\text{mol m}^{-2} \text{s}^{-1}$ versus 0.67 $\mu\text{mol m}^{-2} \text{s}^{-1}$, $p < 0.0001$, $n = 79$). Additionally, the observed temperature sensitivity (Q_{10} of 2.8) is higher than that imposed for soil in Earth system models or reported by arctic experiments warming only the surface. A shoulder-season warming experiment revealed that rapid snow melt, which is becoming a more common event, can result in large methane emissions that may have otherwise been oxidized to carbon dioxide. Thus, warming promotes greenhouse gas emissions from the whole, deepening active layer and may contribute to climate change amplification.

Arctic soils overlying permafrost contain an estimated 900 Pg organic carbon^{1,2}. Much of this carbon is thought to be protected against microbial decomposition by cold temperatures³ and could be mineralized to carbon dioxide (CO₂) and transferred to the atmosphere with a warming climate^{4–7}. Warmer soils may also enhance microbe-driven methane (CH₄) emissions from Arctic soils. Few projections, however, are informed by field-based observations of the direct temperature sensitivity of microbial decomposition and greenhouse gas production. As a result, there is large uncertainty about the magnitude of response and how fast microbial decomposition or ecosystem respiration will change in response to warming.

Climate models predict 3.1–7.7 °C of surface-air warming over permafrost soils by 2100, and warming of the top meter of Cryosol (i.e., permafrost or Gelisol) soils by 3.2–5.8 °C for RCP 4.5 and 8.5, respectively⁸. This warming will have many effects on respiration and greenhouse gas fluxes due to impacts on controls such as microbial community, metabolism, and enzyme activity, substrate availability, and vegetation types and inputs. To represent the direct effect of

warming on microbial respiration, most Earth system models (ESMs) prescribe an apparent temperature sensitivity, or Q_{10} , in their decomposition and respiration modules⁹, but the Q_{10} value is not informed by Arctic observations and is typically a single, common global parameter.

Different approaches to studying the direct effects of temperature on decomposition in Arctic ecosystems, such as incubations, seasonal variation, and in situ manipulative experiments, have different strengths and weaknesses. While incubations are able to control temperature, they do not maintain realistic variations in climate and lack plant inputs that provide microbial substrates^{10,11}. Statistical relationships between ambient (e.g., seasonal) temperature variation and CO₂ or CH₄ fluxes have been used to estimate temperature response functions for those fluxes, but covariation of temperature with plant phenology, insolation, and other ecosystem controls confounds these interpretations and lacks testing. In situ warming experiments take place in the context of realistic climate and vegetation, but have been restricted to locations with sufficient infrastructure (for heating cables

¹Climate and Ecosystem Sciences Division, Berkeley Lab, Berkeley, CA, USA. ²Energy and Resources Group, University of California, Berkeley, CA, USA.

³Wintergreen Earth Science, Kennebunk, ME, USA. ⁴San Francisco Estuary Institute (SFEI), Richmond, CA, USA. ⁵Environmental Studies Program, University of Oregon, Eugene, OR, USA. ⁶College of Urban and Environmental Sciences, Peking University, Beijing, China. ✉e-mail: mstorn@lbl.gov

or infrared lamps for canopy and active-layer warming), low amounts of warming (<1°C), and/or surface soils only (<20 cm, for passive warming with open top chambers, OTCs)^{12,13}. Snow fence and snow relocation experiments have accomplished warmer, deeper heating, but without the ability to control the magnitude of warming¹⁴.

Due to the inherent differences and limitations among these approaches, there are gaps in understanding the response of ecosystem-atmosphere CO₂ and CH₄ fluxes to warming, and varying findings among studies and sites^{12,13}. Therefore, the effects of whole-active-layer warming on Arctic ecosystem carbon fluxes remain highly uncertain.

In the Arctic, soils that are unsaturated with respect to water often overlay saturated horizons that produce large amounts of CH₄, but most of this subsurface CH₄ is oxidized in aerobic layers or microsites rather than emitted to the atmosphere^{15,16}. The microbial processes and soil conditions influencing CH₄ production, consumption, and net fluxes are temperature-sensitive, but few experiments have studied this sensitivity in the field^{17,18}.

An additional need for controlled warming in the field is to investigate the impact of rapid melt of ice or snow over talik areas (thawed zone between the permafrost and the frozen surface). Arctic eddy covariance and chamber measurements have documented pulse releases of CH₄ and CO₂ during the fall and spring shoulder seasons^{19–24}. It is hypothesized that rapid loss of ice or snow cover leads to escape, without opportunities for oxidation, of CH₄ that has accumulated in the subsurface²⁵, and represent an increase in annual ecosystem CH₄ emissions to the atmosphere^{19,22,23,26,27}. Testing this hypothesis in the field would require controlled, rapid warming of the frozen soil surface.

To address these gaps, this study examined the direct effects of active-layer warming and rapid snow/ice melt on ecosystem CO₂ and CH₄ fluxes in continuous permafrost tundra, in Utqiagvik (formerly Barrow), Alaska, using a novel heating approach that achieved controlled warming throughout the active layer while preserving natural climate variation and vegetation inputs (Methods; Supplementary Fig. 1). Based on a recently tested method²⁸, we used heating rods installed vertically in the soil to heat the whole active-layer soil profile to the depth of permafrost (32–44 cm) with control over the amount of warming²⁸. We modified this method to use just one heating rod in the middle of a small treatment plot²⁹, and a photovoltaic system to enable field sites without line power. Greenhouse gas fluxes were measured with a chamber and Los Gatos Research, Inc. Ultraportable Greenhouse Gas Analyzer. We hypothesized that (1) when the whole active layer is warmer, tundra ecosystem respiration rates show higher temperature sensitivity compared to those observed in shallow-warming experiments or imposed (soil) or emergent (soil and plant) in ESMs; (2) using temporal (e.g., seasonal) patterns in temperature and respiration to evaluate temperature sensitivity overestimates the effect of warming relative to using a controlled manipulation that allows comparison of two different temperatures at the same time; and (3) rapid melt of ice or snow allows the release of CH₄ and CO₂ that was produced in underlying thawed (talik) layers.

Results

The solar-powered system was able to heat the whole active layer quickly and maintain the target temperature difference while tracking natural diurnal cycles, for heating during the growing seasons and fall shoulder seasons of 2015–2016 (Fig. 1; Supplementary Fig. 1). To achieve warming consistent with that predicted for 2100, the heated plots were 4.0°C (3.5°C, 4.3°C) median (25th percentile, 75th percentile) warmer based on sensors at the depths at which heating level was regulated (the 10, 20, and 35 cm depths), and 3.8°C (2.8°C, 4.1°C) over all depths (Supplementary Figs. 2 and 3) compared to control plots. At 5, 10, 15, 20, 25, 35, and 50 cm depths respectively, the median and interquartile ranges [median (25th percentile, 75th percentile)] of

heated-control difference were: 1.97 (0.66, 3.19), 3.72 (2.30, 4.23), 4.08 (3.91, 4.80), 4.11 (3.57, 4.61), 4.72 (2.30, 5.31), 4.07 (2.84, 4.57), 1.71 (0.88, 2.40) °C.

There was slightly less warming at 5 cm depth because of rainfall and heat exchange with the atmosphere, and less at the permafrost boundary (50 cm) because energy was consumed by the phase change of thawing permafrost and was advected by lateral flow of the newly thawed water (Fig. 1; Supplementary Figs. 1 and 2). The infrastructure was adequate to heat the soils several degrees warmer if the target warming was set higher.

In the pretreatment phase in 2014–2015 and during unheated periods in 2015, there was no difference in temperature, CO₂ flux, or CH₄ flux between control plots versus plots designated to be heated. Within a few hours of powering the heaters, warming was observed (Supplementary Fig. 1) and CO₂ fluxes in the heated plots increased. During the 2015–2016 warming periods, the warming treatment resulted in a large and significant increase in ecosystem respiration (Fig. 2). (The low vegetative biomass in these systems means that ecosystem respiration and soil respiration rates are similar³⁰, but we refer to ecosystem respiration since the chamber was placed on top of living vegetation.) In both years and all timepoints except October 2015 (when the effect was larger), heating increased ecosystem respiration by nearly 50% over unheated controls ($n=194$ observations; control flux $0.67 \mu\text{mol m}^{-2} \text{s}^{-1}$, heated flux $0.99 \mu\text{mol m}^{-2} \text{s}^{-1}$, treatment difference $p < 0.0001$). There were no differences in temperature and flux rates when heaters were off (Fig. 2), confirming the direct, large effect of heating on belowground respiration processes.

Natural temporal variation in soil temperature was also significantly related to variation in respiration (Fig. 3). The temperature response estimated from natural seasonal variation, however, may be confounded by the covariance of temperature with other factors that influence respiration such as rainfall and plant phenology. Evaluating apparent Q_{10} across both warming treatments and time allowed us to explore how these estimation approaches influence the inferred temperature response. The apparent Q_{10} estimated from the heated-control treatment differences (treatment $Q_{10} = 2.8$, $n = 79$) was lower than that estimated from seasonal temperature variation of (1) the control plots (ambient seasonal $Q_{10} = 6.9$, $n = 79$), or (2) all plots (ambient seasonal $Q_{10} = 4.1$, $n = 168$) (Table 1; Fig. 3). For these cases, Q_{10} was evaluated for time points when the heaters were on. Thus, the temperature response inferred from ambient temperature variation was higher than that for the treatment effect for the same time points. Monthly Q_{10} values are shown in Supplementary Tables 1 and 2 and Supplementary Fig. 4. The average increase in respiration per °C of experimental warming was $0.10 \mu\text{mol m}^{-2} \text{s}^{-1} \text{°C}^{-1}$. Moreover, this treatment-based response rate and the treatment Q_{10} are a conservative estimate of response, since they are based on the warming at 10, 20, and 35 cm depths whereas there was less warming at 5 and 50 cm.

Based on radiocarbon values of respired CO₂, respired carbon from heated plots was older than that from control plots in six out of seven measurements, suggesting that warming resulted in the loss of older ecosystem carbon (Supplementary Table 3, Supplementary Fig. 5), which could be related to the deeper thaw in the heated plots and greater bioavailability of older organic matter at all depths.

Instantaneous measurements of net ecosystem exchange (NEE) were negative (indicating carbon uptake) in both warmed and control plots on 11 of the 14 days on which they were measured (Supplementary Fig. 6), owing to carbon uptake by active vegetation. However, heating reduced net carbon uptake (NEE) slightly but significantly in summer ($P = 0.041$ summer months only, $P = 0.061$ all months; two-tailed paired t-test, Supplementary Fig. 6), accounting for changes in ecosystem respiration and in gross primary productivity, which was slightly higher (more negative) in heated plots ($P = 0.044$ all months).

Methane fluxes were close to zero during the growing season (Fig. 4), consistent with measurements from high-centered and flat-centered polygons in other locations of the Barrow Ecological Observatory (BEO³¹). Heating reduced emissions, shifting the flux from low net emissions to low net uptake, perhaps due to near-surface drying

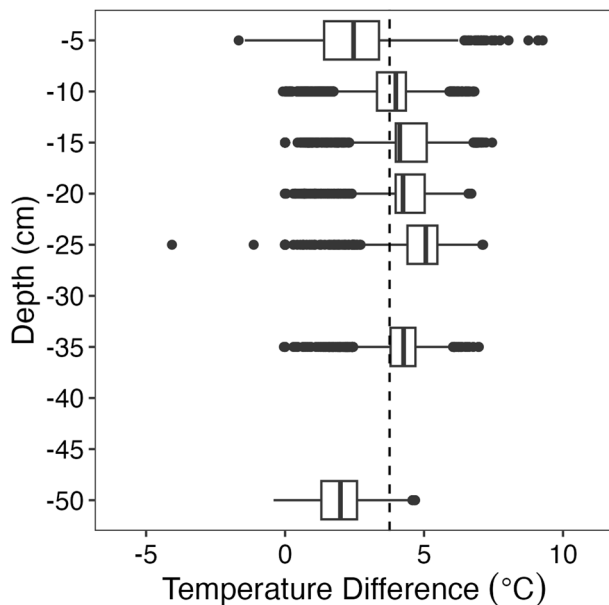


Fig. 1 | The heated-control temperature difference at each depth. The heated-control temperature difference, per depth between 10–50 cm, summarized in boxplots of the difference for each 15-min measurement in all blocks. The vertical dash line represents the median warming for all depths, 3.8 °C. The negative y-axis values indicate depth below the surface (0 cm). Maximum active layer depth was roughly 45 cm in the centers of these polygons. The box reports the median and interquartile range for each depth. For all sensors over the 10–35 cm depth interval, the temperature difference exceeded 2.5 °C 95% of the time; (warming was <2.5 °C for only 5% of the measurements; 8% <3 °C; 14% <3.5 °C). The dates of warming, during growing and fall-shoulder seasons of 2015–2016, are shown in Supplementary Figs. 2 and 3; dates of trace-gas flux measurements are shown in Figs. 2 and 4.

and more oxidation, but the effect was not significant. Globally, non-inundated ecosystems are a sink of about 24 Tg C-CH₄ y⁻¹ for atmospheric CH₄³², and changes in this rate could have a meaningful impact on the global CH₄ methane budget.

Warming the plots during the October shoulder season led to a rapid increase in emissions (Fig. 4). The heaters were off between September 2 and October 14, 2015, allowing the upper 5–10 cm to freeze and a layer of snow and ice to accumulate on the surface. Within 2 days of turning the heaters on October 14, the surface soil warmed enough to partially melt the snow, forming visible holes in the snow and ice cover. This coincided with large releases of CO₂ (Fig. 2) and CH₄ (Fig. 4). CO₂ fluxes from the heated plots increased from 1.37–1.96 μmol m⁻² s⁻¹ over the first 2 days of warming to a rate more than ten times the growing season heated average at 10.08–15.53 μmol m⁻² s⁻¹ the 3rd and 4th days. In contrast, October respiration in the control plots (0.30 μmol m⁻² s⁻¹; n = six sets of measurements over 4 days) was about half what it had been in the growing season. Likewise, CH₄ emissions in heated plots increased to more than 100 times those in the snow-free season (24.53, 27.06, 70.75, and 146.91 μmol m⁻² s⁻¹), whereas control plots had a net CH₄ uptake of -0.12 μmol m⁻² s⁻¹ during the same time period.

Discussion

Belowground warming had a direct, immediate, and large effect on tundra CO₂ production. Respiration sensitivity to experimental warming was high ($Q_{10}=2.8$, $n=79$) in the growing seasons of the 2-year experiment and even higher in the October shoulder season. The effect was detectable within hours of turning the heaters on and remained nearly constant throughout the experiment. This result suggests the enhanced CO₂ production was a direct physiological or thermodynamic response rather than due to ecosystem interactions like changes in nitrogen uptake, root growth, acclimation, substrate availability, or other phenomena emergent after longer-term warming. Increases in root exudation with warming³³ have not been documented in the Arctic.

Several studies have examined the effect of warming on Arctic CO₂ and CH₄ fluxes (e.g.,^{34,35}), including laboratory incubations (e.g.,^{3,10}) and in situ manipulations (e.g.,^{14,36}), but the magnitude and direction of responses vary among studies and sites. A synthesis of laboratory incubations found moderately high (mean $Q_{10}=2.0$, 95% CI 1.8–2.2)

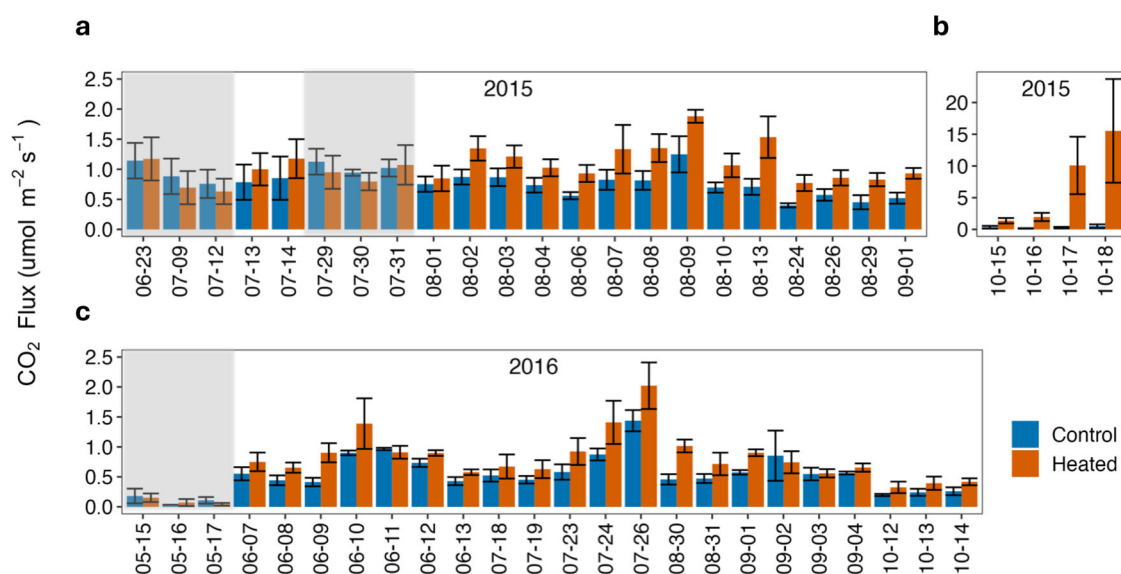


Fig. 2 | Ecosystem respiration in heated and control treatments. Average ecosystem CO₂ respiration for each day of measurement in **a** 2015 June–September, **b** 2015 October shoulder season experiment (note different Y-axis scale), and

c 2016 May–October. Values are averages ± standard error. $N=3-4$ blocks depending on the day. Gray shading indicates periods when the heating treatment was not on (e.g., pre-treatment measurement periods).

temperature sensitivity of CO₂ and CH₄ emissions from permafrost ecosystems¹⁰, but this response is lower than our field results for CO₂ (Q_{10} = 2.8). Similarly, incubations of soil collected near our warming experiment found a 40% increase in heterotrophic respiration due to 5°C warming³. Most incubation studies look at relatively short-term responses, in the absence of plants, typically dominated by fast-cycling carbon pools (e.g.,³⁷). (We consider our field experiment to be relatively short term as well.) Models have been used to infer the dynamics of slow-cycling pools in these studies^{3,38,39}, but these inferences have large uncertainty (ref. 40).

Most in situ manipulative warming experiments in tundra have used the passive warming by OTCs¹², which have a limited effect on deeper soils^{41,42}. The International Tundra Experiment employing growing-season OTCs found moderate, ecosystem-dependent responses of ecosystem respiration to warming in the Arctic tundra (Q_{10} was 1.0–2.0 for dry ecosystems, lower for wet/moist ecosystems⁴³). In contrast, CiPEHR manipulated tundra soil temperatures passively by changing snow depth, and found that warming the whole-active-layer by 1.5°C (5–40 cm depth) led to 20% more growing season respiration⁴⁴. Overall, meta-analysis studies, mainly of passive warming in OTC experiments, showed site-dependent (and minor on average) responses of ecosystem carbon pools or fluxes to warming in Arctic tundra. For example, Crowther et al.⁴⁵, reported large warming-induced losses of soil carbon from carbon-rich

ecosystems (including tundra), but this was not confirmed by an updated analysis⁴⁶ with more sites, particularly in tundra. Similarly, a recent meta-analysis¹² focused on Arctic tundra found a non-significant response of soil respiration and a weak response of ecosystem respiration to warming. Radiocarbon measurements of respired CO₂ during lab incubations have shown that the whole soil profile can contribute to carbon-climate feedback in tundra because deeper and older C has the same temperature sensitivity as shallow and young carbon in the soil profile³. In general, previous field warming experiments that have only warmed surface soils (<20 cm) by a small magnitude (1°C) have likely underestimated the effects of whole-active-layer warming on ecosystem carbon fluxes in the Arctic.

In our study, the temperature sensitivity based on paired measurements from heated and control plots (treatment Q_{10}) was lower than that inferred from ambient seasonal temperature variability (seasonal Q_{10}) at our site. The latter also reflects the covariance of temperature with thaw depth and vegetation carbon inputs over the season⁴⁷. The effect of this covariance has rarely been quantified in the Arctic, but these results suggest that reliance on natural temperature variability overestimates Arctic sensitivity to warming. Nevertheless, even the lower temperature sensitivity of respiration derived from our manipulation was significantly higher than the soil Q_{10} of 1.5–2 imposed in many ecosystem models^{48,49}.

Pulses of CO₂ and CH₄ emissions observed in the Arctic shoulder seasons are hypothesized to be the release of gases, which have accumulated in the talik, due to breaches in surface ice or snow cover²⁵ and references therein). For example, in eddy covariance observations in the BEO, CH₄ release followed a rain-on-snow event. The emitted greenhouse gases in our study had accumulated in the microbially active talik. Due to the timing of release, we concluded that the large pulse of CH₄ and CO₂ emitted in the October shoulder-season experiment was due to the physical effect of heating—melting the ice cap that had formed at the surface while the heaters were off for a month prior to the October warming—rather than to stimulating a very large amount of new microbial production. Climate warming, however, could do both: enhance microbial production in a warmer or long-lasting talik and create more frequent periods of rapid snow- or ice-melt.

Shoulder-season greenhouse-gas releases affect measurement accuracy and the magnitude of annual fluxes. For CO₂, release of talik gases results in large time lags between CO₂ production and release, and occurs outside the growing season when most measurements are made (refs. 19,22,23,26,27), increasing the likelihood of underestimating annual CO₂ emissions. In the case of CH₄, these pulses may allow CH₄ that has accumulated in the subsurface to be released in a manner (i.e., through macro-channels or when methane-oxidizing bacteria are not fully active) that bypasses the CH₄ oxidation that would occur in the growing season. For example, in flat- or high-centered polygons of the BEO, significant amounts of CH₄ are produced in the saturated subsurface but oxidation in the drier surface soils results in very low emission rates that are about 10% of the CH₄

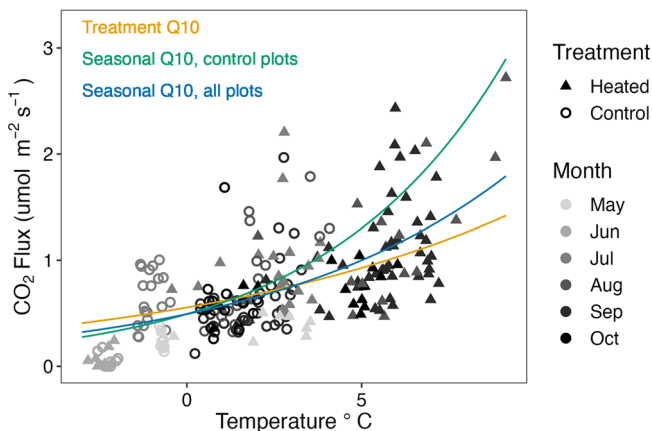


Fig. 3 | Temperature sensitivity of ecosystem respiration based on treatment differences or seasonal variation, in 2015 and 2016 measurement periods.

Respiration versus soil temperature for control (triangle) and heated (circle) plots; shading indicates month. The lines show the CO₂-temperature relationship for the best fit Q_{10} value for (1) Treatment Q_{10} (2.8, yellow line), calculated from heated-control respiration and temperature differences within each block and Eq. 4; (2) Seasonal Q_{10} (6.9, green line) using all control plot data, for days when heaters were on and Eq. 5; and (3) Seasonal Q_{10} (4.4, blue line) using all plots for days when heaters were on. May data were not used in the Q_{10} estimates because there was no heating treatment in that month. Temperature is the average of all 10, 20, and 35 cm sensors in a plot.

Table 1 | The response of surface respiration to soil temperature, quantified by the apparent Q_{10} values and evaluated for the temperature difference in the heating treatment and for the ambient seasonal temperature variation

| | N | Q_{10} | Significance |
|---|-----|----------------|--------------|
| Seasonal Q_{10} . Control plots, for periods when heaters were on | 79 | 6.948 | $P < 0.0001$ |
| Seasonal Q_{10} . Control plots, all time points (heaters on & off) | 98 | 8.512 | $P < 0.0001$ |
| Seasonal Q_{10} . All plots, all time points (heaters on and off) | 209 | 4.352 | $P < 0.0001$ |
| Seasonal Q_{10} . All plots, for periods when heaters were on. | 168 | 4.107 | $P < 0.0001$ |
| Treatment Q_{10} , based on heated-control difference | 79 | Median = 2.798 | |

The fits were non-linear least squares (NLS) for the variation in temperature, using all time points as noted and the treatment combinations shown. The treatment Q_{10} was calculated from the heated and control differences in temperature and respiration each day, using Eq. 4. Data from October 2015 were not included.

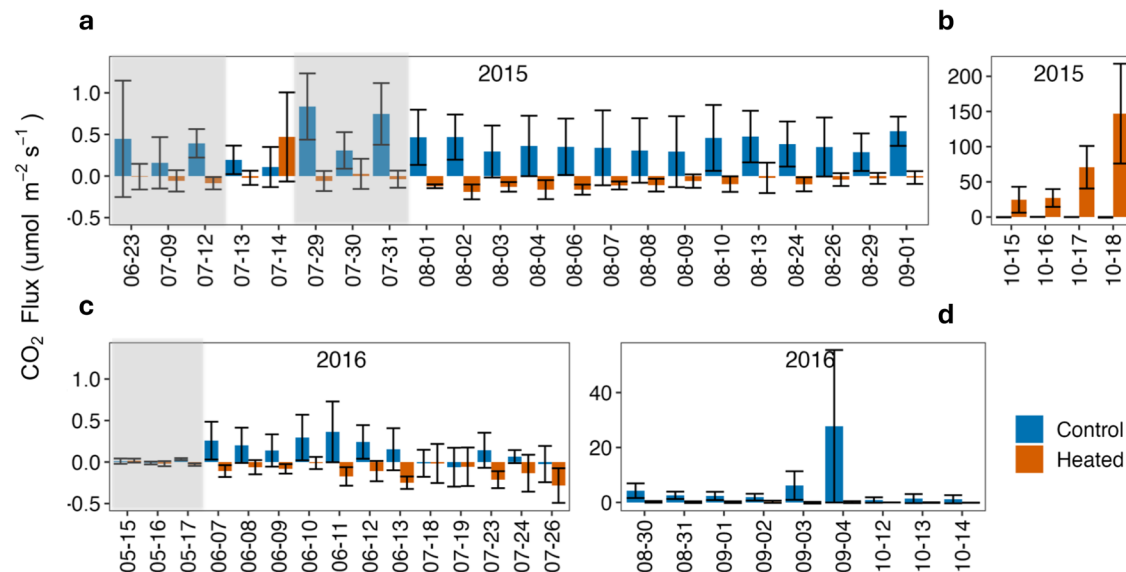


Fig. 4 | Ecosystem CH₄ flux for heated and control treatments. Average CH₄ fluxes for each day of measurement showing difference in CH₄ between heated and control plots in **a** 2015 June–September, **b** 2015 October shoulder season experiment (note different Y-axis scale), **c** 2016 May–July, and **d** 2016 August–October

(note different Y-axis scale). Values are averages \pm standard error of $n = 3$ –4 blocks. Gray shaded areas indicate periods when the heating treatment was not on (e.g., pre-treatment measurement periods).

emissions from inundated sites³¹. Similar observations have been made in other Arctic locations (e.g., Toolik Lake⁵⁰ and others). As a result, the frequency and magnitude of shoulder season gas pulses may influence not only the timing, but also the total amount of annual CH₄ emissions. This mechanism of release of gas trapped in the talik was confirmed by the progressive warming of a large, intact core in the laboratory²⁵. Our study is the first controlled field confirmation of this hypothesis, showing that rapid thaw allows significant CH₄ efflux at sites where the CH₄-carbon would otherwise be oxidized and released as CO₂.

Recent and projected climate trends in the Arctic show more intermittency in ice and snow cover, due to more rain-on-snow events (which have become more common over the past 30 years²⁵, later formation of winter snowpack in fall, and higher frequency of spring warming events. Even steady warming can lead to more freeze-thaw events when superimposed on natural temperature cycles (e.g., bringing the warmer end of the cycle above freezing). These events will lead to higher Arctic CH₄ emissions if, as we observed, they allow soil CH₄ gas to be released to the atmosphere without being oxidized^{31,51}. Development of ESMs is needed to more accurately predict rain-on-snow events and other rapid melt events, as well as to simulate talik formation and the influence of rapid thaw on CH₄ emission vs. oxidation pathways.

This new approach to heating permafrost soil offered three advantages over previous methods. It (1) achieved deeper and greater temperature increases than reported for passive warming, (2) followed natural background temperature and rainfall variability better than snow manipulation or incubations, and (3) allowed for relatively easy setup in remote locations. The single heating rod thawed permafrost and deepened the active layer, but additional power input at depth would have helped achieve the target magnitude of warming at the permafrost boundary, and the addition of an OTC would improve warming of the vegetation and top 5 cm of soil. For the first 2 months, when the experiment was powered by batteries and only operated for about 1 week per month, it was run as a series of short incubation-like studies. Nevertheless, the microclimate of these open-air plots better matched natural variation compared to laboratory incubations, including diurnal temperature cycles and the effects of rain on temperature and moisture. If implemented long term, this experimental approach would likely cause significant subsidence, given the vulnerability of permafrost ground when warmed⁵².

The direct temperature sensitivity quantified by this experiment, an apparent $Q_{10} = 2.8$, is a good test of the prescribed, intrinsic Q_{10} for soil respiration in ESMs. It implies that the direct effects of warming on Arctic CO₂ fluxes may be much larger than are prescribed in current ESMs. For example, in the CESM land model, CLM4.5, the soil decomposition Q_{10} is set to 1.5⁴⁹ and the inferred CCSM4 Q_{10} is 1.9⁹. The inferred Q_{10} is the temperature response that emerges when all internal feedbacks are considered in the ESM simulations, and for CESM was estimated by fitting Eq. 6 to Arctic CO₂ and surface temperature values for four Shared Socioeconomic Pathways (SSPs; see Methods and Supplementary Fig. 7), and is also similar to what has been inferred globally for a range of ESMs^{9,48}.

To explore how our higher value might affect CO₂ fluxes with climate warming in a global model, we projected CO₂ respiration from the global Arctic tundra for 2015–2100, using either the Q_{10} of 2.8 or the inferred ESM Q_{10} of 2 calculated here for CESM (Fig. 5). For the initial fluxes, we used CESM Arctic ecosystem respiration in 2015, and then calculated these fluxes each year based on the Q_{10} (Eq. 6) and CESM soil temperature projections under the four SSPs; Extended Data Fig. 4). We limited our analysis to the tundra land category north of 66°N⁵³. Although ESMs are likely over-simplified, we followed current ESM practice in applying the same Q_{10} pan-Arctic and over the century. The difference in Q_{10} between our experimentally determined value and that imposed a priori implies an additional 2.0–10.2 Pg CO₂ y⁻¹ on average in the period 2080–2100 (with much higher values in 2100), depending on the SSP.

This simplified comparison illustrates the large impact that temperature sensitivity can have on future greenhouse gas fluxes. Moreover, it may be a conservative estimate of the impact since the inferred (i.e., emergent) temperature response of CESM ($Q_{10} = 2$) is higher than CESM's intrinsic (i.e., prescribed for respiration) response ($Q_{10} = 1.5$), suggesting that if CESM implemented the intrinsic ($Q_{10} = 2.8$) measured in this experiment, the inferred, total temperature response of CESM would be even higher. This is not an analysis of long-term or vegetation-driven changes in ecosystem respiration, but rather of the impact of different intrinsic temperature sensitivities on respiration over a warming century. For example, because plant biomass and productivity were held constant, it omits the potential, countervailing impact of decomposition-nitrogen feedbacks that stimulate primary productivity.

Nevertheless, if generalizable, the large temperature response observed here would on balance have significant implications for ecosystem-climate feedbacks. Moreover, we show that long-term or emergent ecosystem changes are not needed to produce a large response.

In conclusion, our findings support the hypotheses that (1) ecosystem respiration in this system is highly sensitive to warming, more

so than current models or shallow warming studies report; (2) the direct effect of controlled warming on respiration is lower than the respiration-temperature relationship derived from seasonal temperature changes, meaning a reliance on ambient temperature variation, e.g., based on seasonal and weather-based variation, overestimates the sensitivity compared to a more controlled approach; and (3) CH₄ produced under the frozen surface of Arctic soils can be released to the atmosphere during rapid melt events in the shoulder seasons, leading to higher CH₄ fluxes by bypassing oxidation pathways that would occur during warmer months. The disparity between the ESM-prescribed temperature sensitivity for ecosystem respiration versus that measured in this controlled field manipulation implies that future carbon fluxes in a warming Arctic may be much larger than previously estimated.

Methods

Site description

The experiment was located in high-centered ice-wedge polygons at the Barrow Environmental Observatory (BEO) near Utqiagvik (formerly Barrow), Alaska (71.3°N, 156.5°W), Fig. 6. Historic (1901–2007) Utqiagvik mean annual temperature is -12 °C and mean annual precipitation is 113.5 mm with a short snow-free summer from June through September⁵⁴. Soils are Cryosols (Gelisols) that are mostly Typic Aquiturbels, Typic Histoturbels, and Typic Aquorthels⁵⁵. Continuous ice-rich permafrost underlies an active layer of 20–60 cm thickness depending on location across the BEO and year. The ice-wedge polygons are discrete landscape units formed from freezing and thawing processes⁵⁶. The high portions of the individual flat- or high-centered polygons, roughly 10 m in diameter and separated by low-lying wet or inundated troughs, had dry, aerobic surface soils and sparse vegetation dominated by *Luzula Arctica*, *Vaccinium vitis idaea*, several moss and lichen species⁵⁷, as well as *Eriophorum vaginatum*, *Petasites frigidus*, *Salix rotundifolia*, and other high arctic tundra species.

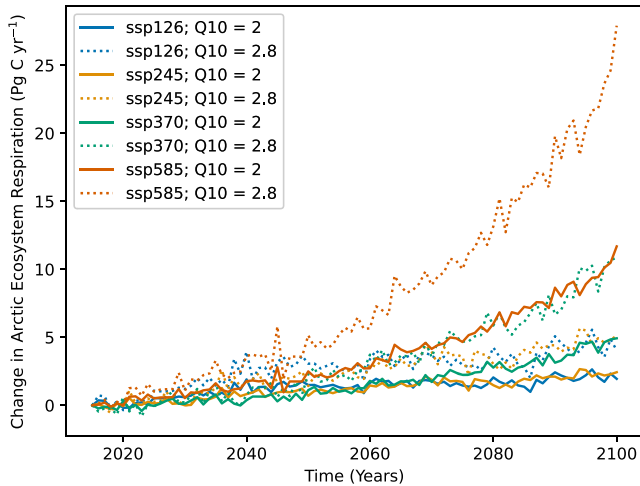


Fig. 5 | The effect of respiration temperature sensitivity on pan-Arctic ecosystem respiration over the 21st century. Annual Arctic-tundra ecosystem respiration from the year 2015 to 2100 calculated using a Q_{10} of 2 (solid lines; the inferred emergent sensitivity of CESM and similar to that of many other ESMs), or a Q_{10} of 2.8 (dashed lines; from this study) and projected temperatures from CESM. The color of the lines refers to the Shared Socioeconomic Pathway scenarios used to determine the change in soil temperature predicted in each year (as shown in Supplementary Fig. 7).

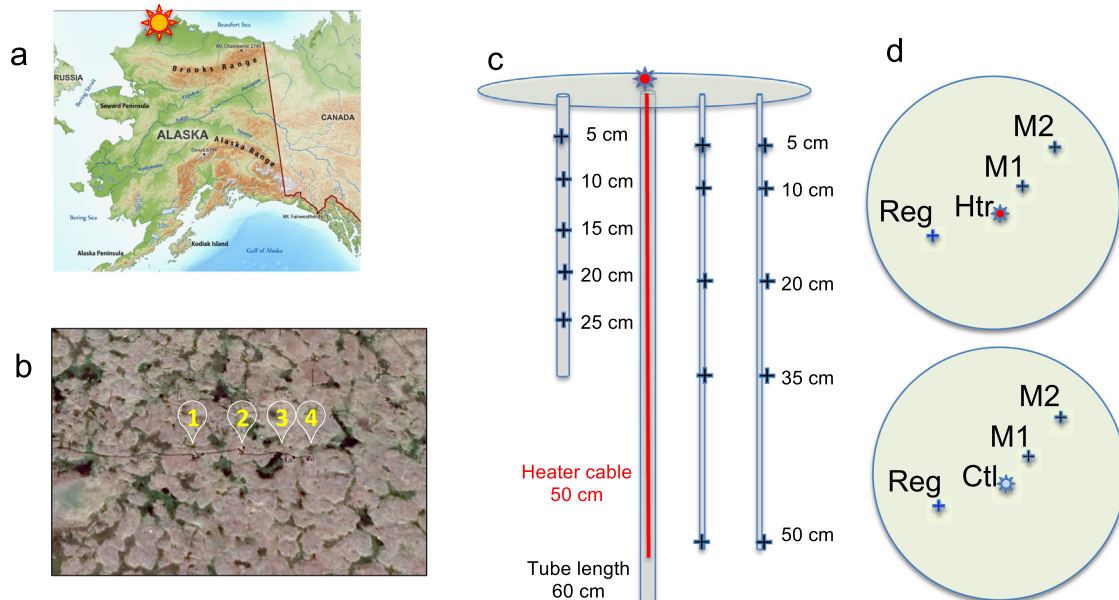


Fig. 6 | Location of tundra-soil warming experiment and schematic for plot infrastructure. **a** Map shows location of Utqiagvik (formerly Barrow), AK, location of the Barrow Environmental Observatory (BEO) on the North Slope of Alaska. Background map credit: <https://www.freeworldmaps.net/united-states/alaska/map.html>. **b** Aerial image of plots on flat-centered polygonal tundra of the BEO. The dark area at base of each white teardrop is one experiment block comprising mesocosms, trail mat, and warming infrastructure. Source of underlying satellite image: Google Earth, July 2016, centered on 71°16'28.88"N, 156°37'59.26"W. Image

© 2024 Maxar Technologies, Image Landsat / Copernicus. **c** Cross-section schematic of experimental plot. Each plot was instrumented with three temperature probes containing five thermistors each and one rod in the center (in heated plots the rod contained heater wire, indicated by red line). The rods were 60 cm long, inserted to a depth of 55 cm. **d** Aerial-view of the 25 cm diameter plots. The monitoring probes were 6 cm (M1) and 10 cm (M2) from the center. The regulator probe (Reg) used to control heating was 8 cm from center.

Table 2 | Summary of belowground soil measurements from soil cores collected in 2014

| Treatment | Date | Depth (cm) | %C | %N | MBC (mg/g) |
|-----------|--------|------------|-------------|---------------|---------------|
| Warming | 8-Sep | 0–10 | 12.1 ± 8.39 | 0.689 ± 0.556 | – |
| | | 10–20 | 8.68 ± 6.05 | 0.499 ± 0.390 | 0.940 ± 1.05 |
| | | 20–30 | 9.22 ± 8.07 | 0.527 ± 0.524 | – |
| | 20-Sep | 0–10 | – | – | – |
| | | 10–20 | 7.82 ± 4.98 | 0.415 ± 0.294 | 0.999 ± 1.19 |
| | | 20–30 | 5.66 ± 2.65 | 0.312 ± 0.175 | – |
| Control | 8-Sep | 0–10 | 16.5 ± 10.8 | 0.658 ± 0.161 | – |
| | | 10–20 | 10.4 ± 4.57 | 0.564 ± 0.291 | 0.818 ± 0.537 |
| | | 20–30 | 11.5 ± 5.79 | 0.611 ± 0.368 | – |
| | 20-Sep | 0–10 | 14.1 ± 4.39 | 0.688 ± 0.208 | – |
| | | 10–20 | 8.96 ± 3.43 | 0.472 ± 0.206 | 0.830 ± 0.662 |
| | | 20–30 | 10.0 ± 6.56 | 0.551 ± 0.404 | – |

Values are averaged across cores collected from six polygons, ($N=6$), including the four polygons used in this experiment. Uncertainty ranges are standard deviations. As described in the text, the warming plots received a low-level glucose addition in 2014, which could not be detected in soil carbon, nitrogen, microbial biomass or ^{13}C that year or in 2015 when the warming experiment started.

Experiment layout and pretreatment measurements

Four blocks were established in the center of four different polygons of roughly equal active layer depth (Fig. 6). On August 24, 2014, we installed two 25 cm diameter mesocosms in each polygon (block) for control and treatment plots. Each mesocosm was created by inserting a 45 cm tall PVC tube (open on top and bottom) vertically in the soil to span the full active layer depth at these sites (32–44 cm measured with a thaw-depth probe adjacent to the plots in 2015–16); each plot was delineated by the 25 cm diameter PVC ring which also isolated the mesocosm soil profile from the surrounding soil. A thicker PVC collar was glued to the top of each mesocosm's PVC column. The collar had a 3 cm deep trench made to seat the CO_2 flux chamber; during measurement, the trench was filled with water to make an airtight seal with the chamber.

The mesocosms were installed the year before the manipulation, to avoid disturbance effects and allow a year of pretreatment fluxes. There was no significant difference between control and pre-heated plots in CO_2 respiration or microbial biomass; aboveground plant biomass was measured near the plots (next section). As part of an earlier study, this site had received a one-time ^{13}C -labeled glucose amendment in 2014 equivalent to 0.1% of the SOC in the top 10 cm, but this carbon addition had no detectable effect on the metrics assessed in this experiment. For example, the glucose amendment had no detectable effect on ecosystem respiration ($P < 0.12$) measured 13 times in 2014 and spring 2015 or soil microbial biomass ($P < 0.11$) measured in fall 2014; we also confirmed that there was also no delayed effect of the amendment in 2016 by monitoring two additional amended polygons outside the heating experiment. We note, however, that residual ^{13}C - CO_2 was detected in 2015 with Keeling plots (Keeling, 1958) in low-glucose-addition plots (glucose addition plots: mean $\delta^{13}\text{C} = 8.55$ per mil, standard deviation = 25.5 per mil, $n = 8$. Control plots: mean $\delta^{13}\text{C} = -23.9$ per mil, standard deviation = 9.97 per mil, $n = 40$). The number of replicate blocks was four in the first year (2015) and first half of 2016 and was reduced to three blocks mid-way through the 2nd year (2016) due to malfunctions in the custom chips controlling the heating and temperature measurements.

Site characterization: soil carbon, microbial biomass, vegetation biomass. We harvested aboveground vegetation in August 2014 from one 25 cm diameter circle per polygon, near the mesocosms. Vegetation was sorted immediately into vascular and nonvascular (moss + lichen) components, oven dried at 60 °C, and weighed

(Supplementary Fig. 8). Live-root biomass, determined in other BEO polygons (for *Carex aquatilis*, *Eriophorum angustifolium*, and *Salix rotundifolia*) is concentrated in the top 25 cm⁵⁸. Soils were sampled from adjacent replicate plots on September 8 and 20, 2014 for analysis of organic carbon and nitrogen content and microbial biomass carbon determined by elemental analysis and chloroform fumigation-extraction, respectively (Table 2).

Warming manipulation

In June 2015, a 60 cm long vertical rod was installed in the center of each heated and control mesocosm (PVC tube). Heater cable in the rod extended 50 cm below the surface. We used a nickel-chrome heating element (Thermosoft Ultra Flexible Cable Heater; www.Thermosoft.net, IT0403-12: 12V, 1.0A, 12WT for 4 ft cable) run in a loop. Resistance was 0.5 ohm per cm for single wire; 1 ohm per cm for the loop. We used KONA 870FT-LV-DP heat-conductive epoxy cement to pot the heater cables in ¼ inch diameter, 0.035 inch wall, 1/8 hard seamless 316 stainless steel tubes. An insulated crimp connector at the bottom of the heater made the electrical turnaround inside the rod. Disturbance-control rods were constructed in the same way but without heater wire and installed into control plots. The layout of the heating rod and temperature probes is shown in Fig. 6.

The temperature probes and heating rods were installed by drilling a pilot hole (1.5–3.5 mm larger in diameter than the probe or rod), into the frozen permafrost (using a cordless rotary hammer drill (Bosch 36 V Li-Ion) and custom-length drill bits) and then inserting the probe or rod to the desired depth.

Temperature monitoring and heating regulation. Three temperature probes were inserted into each plot, at 6, 8, and 10 cm from the center of the plot (where the heating or disturbance-control rod was). The custom-made probes contained five thermistors between 5–50 cm depth (Fig. 6). The thermistors were glued along a nylon strip that was inserted into a butyrate tube, and the tube was filled with urethane. An improved version is documented in Léger et al.⁵⁹.

Temperature and heating status (on/off) were logged and saved every 3 s in 2015 as we evaluated the system, and every 30 s in 2016 until mid-June and then at 5-min intervals for the rest of the season to save on memory. The probes at 8 cm distance from center (hereafter regulator probes) were used to control the heating. At each timepoint, if the depth-averaged temperature difference between regulator probes in a heated and unheated plot pair was < 4 °C, the heater was turned on until the next measurement time point (e.g., 3 s) and re-evaluated. If the temperature difference was ≥ 4 °C, the heating rod received no power. The temperature readings were aggregated to 1- or 2-h averages for plots and analysis.

The single vertical heating rod was able to warm the whole active layer and maintain the target temperature difference (Fig. 2). We maintained a temperature difference of 4.0 °C based on sensors averaged over 10, 20, and 35 cm depths (Fig. 1; Supplementary Figs. 2 and 3), and 3.8 °C median over all depths. The amount of warming at 5 cm depth was more variable and rarely reached 4 °C because of rainfall and heat exchange with the atmosphere. Peak active-layer depth averaged < 50 cm in unheated soil, based on thaw depth probes and temperature sensors; in the absence of heating, 50 cm temperatures were < 0 °C (Fig. 2; Supplementary Fig. 3). Heating brought the 50 cm temperature above 0 °C, indicating thaw of frozen ground and a deeper active layer. The temperature difference at 50 cm between treatments was less than 4 °C because energy was consumed by the phase change of thawing water in permafrost and energy could be advected by lateral flow of the newly thawed water (Fig. 1). For these reasons, average warming of the whole profile over all depths and plot area (all probes) was always lower than the set target of 4 °C. The infrastructure was adequate to heat the soils several degrees warmer if desired, however, by adjusting the heater settings.

Power. From June 27 to August 11, 2015, the heaters, temperature probes, and dataloggers were powered by two 12 V 110 amp-hour marine batteries. Drained batteries were swapped manually for charged units; thus, heating occurred only when the research team was in Utqiagvik. After August 12, 2015, power was supplied by photovoltaic panels and the experiment operated nearly continuously during the growing season. For each block, two 123 W panels (Sharp ND-123UJF; 662 × 1499 mm) were connected to a charge controller to maintain charge on the batteries. The panels were mounted to a Unistrut frame anchored to permafrost, facing south at a -70° angle to the horizontal.

To minimize power requirements, custom-made circuit boards controlled the warming and logged the data. Each board sampled and digitized 16 analog thermistor channels with a 24-bit analog-to-digital converter (ADS1243). Data were streamed via RS232/RS485 and WiFi as well as stored locally on three 1 Gbit NAND flash chips. A low power Microchip microcontroller (PIC18F97J60) contained the firmware to control data acquisition, storage, communication, and control of the heater circuit. If a controller system malfunctioned, data from that block were not used for the time period that the heating or temperature monitoring were not operational. The interface for setup of system properties, deployment, and data downloading was initially via a custom iOS App running on an iPad. This was upgraded to a Gumstix Overo embedded Linux module and a Node.js web application to allow for a simplified interface and connection to a WiFi or wired network.

Carbon fluxes and flux isotopes

Surface fluxes of CO₂ and CH₄. Surface fluxes of CO₂ and CH₄ were measured using chambers 25 cm in diameter, vented to minimize pressure excursions due to the Venturi effect⁶⁰, circulating through a Los Gatos Research, Inc. (LGR) Ultra-Portable Greenhouse Gas Analyzer (915-0011). We used opaque chambers to measure ecosystem respiration (surface respiration or R_{eco}) and CH₄ flux. We monitored headspace concentrations for 3–7 min and calculated the flux rate from the linear region of the concentration vs. time curve. Immediately prior to measuring respiration on some days, we measured fluxes with a clear chamber, to estimate NEE using the first 60 s of each measurement; after 60 s the drawdown rate decreased, possibly due to the drawdown of CO₂ mixing ratios in the chamber or to fogging due to evapotranspiration. Flux measurements were measured before (2014, 2015) and during heating treatments in 2015 and 2016 (see Fig. 2 and Methods Section 2. “Experiment layout and pretreatment measurements”).

Radiocarbon (¹⁴C) of soil respiration. On August 5 and 30 in 2015 and May 23 and June 12, 2016, we collected CO₂ from non-vented soil chambers for radiocarbon analysis. Samples were collected when the heaters were on. Briefly, after circulating chamber gas through soda lime for 20 min to remove CO₂, we allowed CO₂ to accumulate over 2–24 h, depending on the CO₂ flux rate. Prior to sampling, we measured the CO₂ concentration in the chamber by passing 30 mL of gas through a LI-820 CO₂ gas analyzer (LI-COR, Inc.). Samples were collected in one or more 500–1000 mL evacuated stainless steel canisters connected to chamber sampling ports via capillary tubing. For atmospheric radiocarbon values we collected local air samples in 3000 mL stainless steel canisters on August 30, 2015, and May 25, 2016.

The CO₂ from gas samples was cryogenically purified under vacuum, split for ¹⁴C and ¹³C analysis, and sealed in 6 mm quartz tubes at Berkeley Lab. Samples were analyzed at the Lawrence Livermore National Lab Center for Accelerator Mass Spectrometry, where CO₂ was reduced to graphite on iron powder under H₂⁴⁸ and ¹⁴C abundance measured using a HVEC FN Tandem Van de Graaff accelerator mass spectrometer. ¹³C/¹²C was analyzed on the UC Davis Stable Isotope Laboratory GVI Optima Stable Isotope Ratio Mass Spectrometer. Radiocarbon content $\Delta^{14}C$ is reported as fraction of the modern NBS Oxalic Acid I (OX1) standard ($F^{14}C$), and as deviations in parts per thousand (‰) from the absolute (decay-corrected) OX1 standard

($\Delta^{14}C$), following Stuiver and Polach (1977)⁴⁹. Values have been corrected for mass-dependent isotopic fractionation using ¹³C measurements of the splits.

We corrected surface chamber radiocarbon measurements for atmospheric contamination (e.g., residual atmospheric air in the chamber headspace after scrubbing) using a previously published method⁶¹. Briefly, we determined the fractional contributions of background atmosphere and ecosystem respiration to the measured chamber gas using two-member mixing models with measured $\delta^{13}C$ and $\Delta^{14}C$ values as shown:

$$\delta^{13}C_M = f_{atm}(-9.23\text{‰}) + f_R(-24.41\text{‰}) \quad (1)$$

$$\Delta^{14}C_M = f_{atm}(\Delta^{14}C_{atm}) + f_R(\Delta^{14}C_R) \quad (2)$$

$$f_R + f_{atm} = 1 \quad (3)$$

Subscripts for M , atm , and R denote measured, atmospheric, and respired (net surface exchange), respectively. In 2015 and 2016, $\Delta^{14}C_{atm} = 15.1\text{‰}$ and 10.1‰ respectively. These values were consistent with the Arctic atmospheric radiocarbon record and its recent 2–3‰ annual decrease⁶², with BEO values in the three preceding years of 22.2‰ (2012), 19.3‰ (2013), and 17.8‰ (2014). The $\delta^{13}C$ of respiration (-24.41‰) was estimated as the minimum value (i.e., least atmospheric contamination) of the 12 plot measurements.

Data analysis and statistics: estimating Q_{10} and E_a

The effect of heating and the temperature sensitivity of CO₂ and CH₄ fluxes were calculated using measurements from which October 2015 (shoulder season experiment) were excluded. The warming treatment effect was evaluated with a mixed linear effects model, with block as a random factor (package nlme, <https://cran.r-project.org/web/packages/nlme/citation.html>, R Version 4.0.4). Treatment-effect Q_{10} was calculated as in⁶³,

$$Q_{10} = \frac{R_H}{R_C}^{10/(T_H - T_C)} \quad (4)$$

Where R is the CO₂ production rate from the heated (subscript H) or control (subscript C) plots, and T is the corresponding temperature from the heated or control plots.

To estimate the response to natural temporal variation in temperature, we fit both a non-linear least squares (NLS; Eq. 5) and a linear (Eq. 6) regression relationship relating the observed temperature to the CO₂ production rate. We fit two parameters, (R_0 and k) in Eq. 5 or the equivalent (a and b) in Eq. 6, and the Q_{10} is a function of k (or b).

$$(R = R_0 e^{kT}; \text{ and } Q_{10} = e^{10k}) \quad (5)$$

$$\log(R) = a + bT, \text{ and } Q_{10} = e^{10b} \quad (6)$$

We report the results of the NLS because it had lower residual standard error.

We also expressed the temperature sensitivity of CO₂ production rate using the Arrhenius equation,

$$R = \alpha e^{-E_a/RT} \quad (7)$$

Where α is the pre-exponential constant, E_a is the activation energy, and R is the universal gas constant. The activation energy is the minimum amount of energy needed for a chemical reaction. Similar to k (or b) in Eqs. 5 and 6, E_a is related to the temperature sensitivity, where reactions with high E_a are more temperature sensitive.

Data analysis and statistics: estimating effect of Q_{10} on projected pan-Arctic CO₂ respiration

To estimate how much more CO₂ release would be expected from our measured temperature sensitivity compared to the commonly imposed Q_{10} of 2, we conducted a scaling exercise using model output from the Community ESM version 2. Model output was accessed from the Earth System Grid Federation (esgf-node.llnl.gov/search/cmip6). We downloaded CESM ScenarioMIP runs ssp126, ssp245, ssp370, ssp585, using realization r11i1p1f1 for the years 2015–2100 for all scenarios. Time series were originally monthly, but the months June, July, and August were averaged annually to create a time series where each year represents the temperature or ecosystem respiration of the 3-month growing season during which measurements were taken in this study.

Arctic tundra was subsetted using the map from the National Snow and Ice Data Center³³, which was downloaded in 2.5 arcmin resolution and coarsened to fit the CESM model native 0.9×1.25 finite volume grid (192×288 latxlon) by assigning the larger CESM grid cell as tundra if the majority of higher resolution map grid cells in the defined area were tundra.

Modeled (CESM) soil temperature (Supplementary Fig. 7) was averaged across depth increments using weights fitted using an optimization function so that the average of the weighted depth increments was equal to the average of the measurement depth increments (taken at 10, 20, and 35 cm). Ecosystem respiration was calculated as the sum of autotrophic and heterotrophic respiration variables. Values were scaled up by multiplying the respiration rate for each grid cell by the ice-free land area of each grid cell and summing across latitude and longitude. The changes in soil temperature and ecosystem respiration were calculated by subtracting the soil temperature (or ecosystem respiration) in each year from the soil temperature (or respiration) in 2015, respectively. We estimated the apparent temperature sensitivity of ecosystem respiration predicted by CESM by fitting Eq. 6, where R = ecosystem respiration, and T = soil temperature averaged to match the depth increments from this study. This fit yields the same two parameters described in Eq. 5: the slope k which can be used to calculate Q_{10} , and the intercept R_0 . Inferred Q_{10} using this fitting method ranged from 1.7 to 1.9 globally and from 1.8 to 2.6 in the Arctic tundra, depending on the SSP scenario. Using the fitted R_0 for each SSP scenario and setting Q_{10} to values we are interested in, e.g., $Q_{10} = 2$ (to match the average Q_{10} across SSP scenarios for Arctic tundra), $Q_{10} = 2.8$ (to match the experiment results), we can estimate what the ecosystem respiration would be for each scenario with a given inferred long-term Q_{10} . This inferred Q_{10} is not equivalent to the intrinsic Q_{10} of soil decomposition in the model, since the former includes the temperature sensitivity of other ecosystem processes that change with warming and over time (e.g., changes in plant inputs). Typically, the intrinsic Q_{10} (CLM4.5 $Q_{10} = 1.5$)⁴⁹ is lower than the apparent Q_{10} (CCSM4 $Q_{10} = 1.9$)⁴⁸. Thus, assuming the apparent Q_{10} of the Arctic is 2.8 likely gives a conservative estimate of respiration, meaning that the amount of carbon released in Fig. 5 for $Q_{10} = 2.8$ is likely much less than the amount of carbon released if we had set the intrinsic Q_{10} of the model to 2.8.

Data availability

The data generated in this study have been deposited in ESS-DIVE, a public database supported by the U.S. Department of Energy, Office of Science, Office of Biological and Environmental Research, and are openly accessible under <https://doi.org/10.15485/2475418>.

References

- Hugelius, G. et al. Improved estimates show large circumpolar stocks of permafrost carbon while quantifying substantial uncertainty ranges and identifying remaining data gaps. *Biogeosci. Discuss.* **11**, 4771–4822 (2014).
- Mishra, U. et al. Spatial heterogeneity and environmental predictors of permafrost region soil organic carbon stocks. *Sci. Adv.* **7**, eaaz5236 (2021).
- Vaughn, L. J. S. & Torn, M. S. 14C evidence that millennial and fast-cycling soil carbon are equally sensitive to warming. *Nat. Clim. Chang.* **9**, 467–471 (2019).
- Schuur, E. A. G. et al. Expert assessment of vulnerability of permafrost carbon to climate change. *Clim. Chang.* **119**, 359–374 (2013).
- McGuire, A. D. et al. Dependence of the evolution of carbon dynamics in the northern permafrost region on the trajectory of climate change. *Proc. Natl. Acad. Sci. USA.* **115**, 3882–3887 (2018).
- Natali, S. M., Schuur, E. A. G., Webb, E. E., Pries, C. E. H. & Crummer, K. G. Permafrost degradation stimulates carbon loss from experimentally warmed tundra. *Ecology* **95**, 602–608 (2014).
- Dorrepaal, E. et al. Carbon respiration from subsurface peat accelerated by climate warming in the subarctic. *Nature* **460**, 616–619 (2009).
- Soong, J. L., Phillips, C. L., Ledna, C., Koven, C. D. & Torn, M. S. CMIP5 models predict rapid and deep soil warming over the 21st century. *J. Geophys. Res. Biogeosci.* **125**, e2019JG005266 (2020).
- Todd-Brown, K. E. O. et al. Causes of variation in soil carbon simulations from CMIP5 Earth system models and comparison with observations. *Biogeosciences* **10**, 1717–1736 (2013).
- Schädel, C. et al. Potential carbon emissions dominated by carbon dioxide from thawed permafrost soils. *Nat. Clim. Chang.* **6**, 950–953 (2016).
- Torn, M. S. et al. A call for international soil experiment networks for studying, predicting, and managing global change impacts. *SOIL Discuss.* **2**, 133–151 (2015).
- Pold, G., Baillargeon, N., Lepe, A., Rastetter, E. B. & Sistla, S. A. Warming effects on arctic tundra biogeochemistry are limited but habitat-dependent: a meta-analysis. *Ecosphere* **12**, e03777 (2021).
- Yan, W., Zhong, Y., Yang, J., Shanguan, Z. & Torn, M. S. Response of soil greenhouse gas fluxes to warming: a global meta-analysis of field studies. *Geoderma* **419**, 115865 (2022).
- Plaza, C. et al. Direct observation of permafrost degradation and rapid soil carbon loss in tundra. *Nat. Geosci.* **12**, 627–631 (2019).
- Whalen, S. C., Reeburgh, W. S. & Sandbeck, K. A. Rapid methane oxidation in a landfill cover soil. *Appl. Environ. Microbiol.* **56**, 3405–3411 (1990).
- Whalen, S. C., Reeburgh, W. S. & Reimers, C. E. Control of tundra methane emission by microbial oxidation. in *Landscape Function and Disturbance in Arctic Tundra* (eds. Reynolds, J. F. & Tenhunen, J. D.) 257–274 (Springer Berlin Heidelberg, 1996).
- Lamb, E. G. et al. A High Arctic soil ecosystem resists long-term environmental manipulations. *Glob. Chang. Biol.* **17**, 3187–3194 (2011).
- Voigt, C. et al. Warming of subarctic tundra increases emissions of all three important greenhouse gases—carbon dioxide, methane, and nitrous oxide. *Glob. Chang. Biol.* **23**, 3121–3138 (2017).
- Zona, D. et al. Cold season emissions dominate the Arctic tundra methane budget. *Proc. Natl. Acad. Sci. USA.* **113**, 40–45 (2016).
- Fahnestock, J. T., Jones, M. H. & Welker, J. M. Wintertime CO₂ efflux from Arctic soils: Implications for annual carbon budgets. *Global Biogeochem. Cycles* **13**, 775–779 (1999).
- Bubier, J., Crill, P. & Mosedale, A. Net ecosystem CO₂ exchange measured by autochambers during the snow-covered season at a temperate peatland. *Hydrol. Process.* **16**, 3667–3682 (2002).
- Hargreaves, K. J., Fowler, D., Pitcairn, C. E. R. & Aurela, M. Annual methane emission from Finnish mires estimated from eddy covariance campaign measurements. *Theor. Appl. Climatol.* **70**, 203–213 (2001).
- Wille, C., Kutzbach, L., Sachs, T., Wagner, D. & Pfeiffer, E.-M. Methane emission from Siberian arctic polygonal tundra: eddy

- covariance measurements and modeling. *Glob. Chang. Biol.* **14**, 1395–1408 (2008).
24. Oechel, W. C., Laskowski, C. A., Burba, G., Gioli, B. & Kalhori, A. A. M. Annual patterns and budget of CO₂ flux in an Arctic tussock tundra ecosystem. *J. Geophys. Res. Biogeosci.* **119**, 323–339 (2014).
 25. Raz-Yaseef, N. et al. Large CO₂ and CH₄ emissions from polygonal tundra during spring thaw in northern Alaska. *Geophys. Res. Lett.* **44**, 504–513 (2017).
 26. Mastepanov, M. et al. Revisiting factors controlling methane emissions from high-arctic tundra. *Biogeosci. Discuss.* **9**, 15853–15900 (2012).
 27. Tagesson, T. et al. Land-atmosphere exchange of methane from soil thawing to soil freezing in a high-Arctic wet tundra ecosystem. *Glob. Chang. Biol.* **18**, 1928–1940 (2012).
 28. Hanson, P. J. et al. A method for experimental heating of intact soil profiles for application to climate change experiments. *Glob. Chang. Biol.* **17**, 1083–1096 (2011).
 29. Castanha, C., Zhu, B., Hicks Pries, C. E., Georgiou, K. & Torn, M. S. The effects of heating, rhizosphere, and depth on root litter decomposition are mediated by soil moisture. *Biogeochemistry* **137**, 267–279 (2018).
 30. Ge, L., Lafleur, P. M. & Humphreys, E. R. Respiration from soil and ground cover vegetation under tundra shrubs. *Arct. Antarct. Alp. Res.* **49**, 537–550 (2017).
 31. Vaughn, L. J. S., Conrad, M. E., Bill, M. & Torn, M. S. Isotopic insights into methane production, oxidation, and emissions in Arctic polygonal tundra. *Glob. Chang. Biol.* **22**, 3487–3502 (2016).
 32. Saunio, M. et al. The global methane budget 2000–2017. *Earth Syst. Sci. Data* **12**, 1561–1623 (2020).
 33. Heinzle, J. et al. Increase in fine root biomass enhances root exudation by long-term soil warming in a temperate forest. *Front. For. Glob. Chang.* **6**, 1152142 (2023).
 34. Shaver, G. R. et al. Global Warming and Terrestrial Ecosystems: A Conceptual Framework for Analysis: Ecosystem responses to global warming will be complex and varied. Ecosystem warming experiments hold great potential for providing insights on ways terrestrial ecosystems will respond to upcoming decades of climate change. Documentation of initial conditions provides the context for understanding and predicting ecosystem responses. *Bioscience* **50**, 871–882 (2000).
 35. Schuur, E. A. G. et al. Climate change and the permafrost carbon feedback. *Nature* **520**, 171–179 (2015).
 36. Sistla, S. A. et al. Long-term warming restructures Arctic tundra without changing net soil carbon storage. *Nature* **497**, 615–618 (2013).
 37. Torn, M. S., Vitousek, P. M. & Trumbore, S. E. The influence of nutrient availability on soil organic matter turnover estimated by incubations and radiocarbon modeling. *Ecosystems* **8**, 352–372 (2005).
 38. Schädel, C. et al. Circumpolar assessment of permafrost C quality and its vulnerability over time using long-term incubation data. *Glob. Chang. Biol.* **20**, 641–652 (2014).
 39. Torn, M. S., Swanston, C. W., Castanha, C. & Trumbore, S. E. in *Biophysico-Chemical Processes Involving Natural Nonliving Organic Matter in Environmental Systems* 219–272 (Wiley, 2009).
 40. Bouskill, N. J., Riley, W. J., Zhu, Q., Mekonnen, Z. A. & Grant, R. F. Alaskan carbon-climate feedbacks will be weaker than inferred from short-term experiments. *Nat. Commun.* **11**, 5798 (2020).
 41. Marion, G. M. et al. Open-top designs for manipulating field temperature in high-latitude ecosystems. *Glob. Chang. Biol.* **3**, 20–32 (1997).
 42. Hollister, R. D. et al. A review of open top chamber (OTC) performance across the ITEX Network. *Arct. Sci.* **9**, 331–344 (2023).
 43. Oberbauer, S. F. et al. Tundra CO₂ fluxes in response to experimental warming across latitudinal and moisture gradients. *Ecol. Monogr.* **77**, 221–238 (2007).
 44. Natali, S. M. et al. Effects of experimental warming of air, soil and permafrost on carbon balance in Alaskan tundra. *Glob. Chang. Biol.* **17**, 1394–1407 (2011).
 45. Crowther, T. W. et al. Quantifying global soil carbon losses in response to warming. *Nature* **540**, 104–108 (2016).
 46. van Gestel, N. et al. Predicting soil carbon loss with warming. *Nature* **554**, E4–E5 (2018).
 47. Carey, J. C. et al. Temperature response of soil respiration largely unaltered with experimental warming. *Proc. Natl. Acad. Sci. USA.* **113**, 13797–13802 (2016).
 48. Todd-Brown, K., Zheng, B. & Crowther, T. W. Field-warmed soil carbon changes imply high 21st-century modeling uncertainty. *Biogeosciences* **15**, 3659–3671 (2018).
 49. Lawrence, D. M., Koven, C. D., Swenson, S. C., Riley, W. J. & Slater, A. G. Permafrost thaw and resulting soil moisture changes regulate projected high-latitude CO₂ and CH₄ emissions. *Environ. Res. Lett.* **10**, 094011 (2015).
 50. Torn, M. S. & Chapin, F. S. Environmental and biotic controls over methane flux from Arctic tundra. *Chemosphere* **26**, 357–368 (1993).
 51. Throckmorton, H. M. et al. Pathways and transformations of dissolved methane and dissolved inorganic carbon in Arctic tundra watersheds: Evidence from analysis of stable isotopes. *Global Biogeochem. Cycles* **29**, 1893–1910 (2015).
 52. Rodenhizer, H. et al. Carbon thaw rate doubles when accounting for subsidence in a permafrost warming experiment. *J. Geophys. Res. Biogeosci.* **125**, e2019JG005528 (2020).
 53. Liston, G. Global Seasonal-Snow Classification, Version 1. NASA National Snow and Ice Data Center Distributed Active Archive Center. <https://doi.org/10.5067/99FTCYYYLAQO> (2021).
 54. Hubbard, S. S. et al. Quantifying and relating land-surface and subsurface variability in permafrost environments using LiDAR and surface geophysical datasets. *Hydrogeol. J.* **21**, 149–169 (2013).
 55. Bockheim, J. G., Everett, L. R., Hinkel, K. M., Nelson, F. E. & Brown, J. Soil organic carbon storage and distribution in arctic tundra, Barrow, Alaska. *Soil Sci. Soc. Am. J.* **63**, 934–940 (1999).
 56. Billings, W. D. & Peterson, K. M. Vegetational change and ice-wedge polygons through the thaw-lake cycle in arctic Alaska. *Arct. Alp. Res.* **12**, 413–432 (1980).
 57. Sloan, V. et al. Plant community composition and vegetation height, Barrow, Alaska, Ver. 1. <https://doi.org/10.5440/1129476> (2014).
 58. Zhu, Q., Iversen, C. M., Riley, W. J., Slette, I. J. & Vander Stel, H. M. Root traits explain observed tundra vegetation nitrogen uptake patterns: Implications for trait-based land models: Tundra N Uptake Model-Data Comparison. *J. Geophys. Res. Biogeosci.* **121**, 3101–3112 (2016).
 59. Léger, E. et al. A distributed temperature profiling method for assessing spatial variability in ground temperatures in a discontinuous permafrost region of Alaska. *The Cryosphere* **13**, 2853–2867 (2019).
 60. Xu, L. et al. On maintaining pressure equilibrium between a soil CO₂ flux chamber and the ambient air. *J. Geophys. Res.* <https://doi.org/10.1029/2005JD006435> (2006).
 61. Schuur, E. A. G. & Trumbore, S. E. Partitioning sources of soil respiration in boreal black spruce forest using radiocarbon: isotope partitioning of soil respiration. *Glob. Chang. Biol.* **12**, 165–176 (2006).
 62. Vaughn, L. & Torn, M. Radiocarbon measurements of ecosystem respiration and soil pore-space CO₂ in Utqiagvik (Barrow), Alaska. *Earth Syst. Sci. Data* <https://doi.org/10.5194/ESSD-10-1943-2018> (2018).
 63. Hicks Pries, C. E., Castanha, C., Porras, R. C. & Torn, M. S. The whole-soil carbon flux in response to warming. *Science* **355**, 1420–1423 (2017).

Acknowledgements

We thank the UIC Science Native Corporation for facilitating our scientific research on the Barrow Environmental Observatory, which is Iñupiat land. The Next-Generation Ecosystem Experiments (NGEE Arctic) project is supported by the Office of Biological and Environmental Research in the DOE Office of Science. The Berkeley Lab Belowground Biogeochemistry Science Focus Area and Geophysical Measurement Facility are supported by the U.S. Department of Energy, Office of Science, Office of Biological and Environmental Research under contract number DE-AC02-05CH11231.

Author contributions

M.S.T. conceived of and designed warming experiment. Set up and performed experiment and collected field data. Analyzed data and made preliminary figures. Wrote first draft of manuscript. R.Z.A. analyzed data, produced graphical elements, and contributed to manuscript. L.J.S.V. set up and performed pretreatment experiments, characterized the field site with field and laboratory data, processed and analyzed experiment data, and contributed to manuscript. O.C. co-designed and set up experiment infrastructure, performed field warming experiment, collected data in the field, and contributed to manuscript. J.B.C. co-designed and set up experiment infrastructure, performed field warming experiment, collected data in the field, and contributed to manuscript. B.Z. set up and performed pretreatment experiments in the field and contributed to manuscript.

Competing interests

The authors declare no competing interests.

Additional information

Supplementary information The online version contains supplementary material available at <https://doi.org/10.1038/s41467-024-54990-9>.

Correspondence and requests for materials should be addressed to Margaret S. Torn.

Peer review information *Nature Communications* thanks Liam Hefferman, Xiaodong Wu and the other, anonymous, reviewers for their contribution to the peer review of this work. A peer review file is available.

Reprints and permissions information is available at <http://www.nature.com/reprints>

Publisher's note Springer Nature remains neutral with regard to jurisdictional claims in published maps and institutional affiliations.

Open Access This article is licensed under a Creative Commons Attribution-NonCommercial-NoDerivatives 4.0 International License, which permits any non-commercial use, sharing, distribution and reproduction in any medium or format, as long as you give appropriate credit to the original author(s) and the source, provide a link to the Creative Commons licence, and indicate if you modified the licensed material. You do not have permission under this licence to share adapted material derived from this article or parts of it. The images or other third party material in this article are included in the article's Creative Commons licence, unless indicated otherwise in a credit line to the material. If material is not included in the article's Creative Commons licence and your intended use is not permitted by statutory regulation or exceeds the permitted use, you will need to obtain permission directly from the copyright holder. To view a copy of this licence, visit <http://creativecommons.org/licenses/by-nc-nd/4.0/>.

© The Author(s) 2024